Tetrahedral Chain Order in the $Sr_2Fe_2O_5$ Brownmillerite

Hans D'Hondt,*,† Artem M. Abakumov,†,‡ Joke Hadermann,† Anna S. Kalyuzhnaya,‡ Marina G. Rozova,‡ Evgeny V. Antipov,‡ and Gustaaf Van Tendeloo†

EMAT, University of Antwerp, Groenenborgerlaan 171, B-2020 Antwerp, Belgium, and Department of Chemistry, Moscow State University, 119992 Moscow, Russia

Received June 25, 2008. Revised Manuscript Received September 22, 2008

The crystal structure of the $Sr_2Fe_2O_5$ brownmillerite has been investigated using electron diffraction and high resolution electron microscopy. The $Sr_2Fe_2O_5$ structure demonstrates two-dimensional order: the tetrahedral chains with two mirror-related configurations (L and R) are arranged within the tetrahedral layers according to the −L−R−L−R− sequence, and the layers themselves are displaced with respect to each other over 1/2[111] or 1/2[11$\bar{1}$] vectors of the brownmillerite unit cell, resulting in different ordered stacking variants. A unified superspace model is constructed for ordered stacking sequences in brownmillerites based on the average brownmillerite structure with $a = 5.5298(4)$Å, $b = 15.5875(12)$Å, $c = 5.6687(4)$Å, and (3 + 1)-dimensional superspace group $I2/m(0\beta\gamma)0s$, $\mathbf{q} = \beta\mathbf{b}^* + \gamma\mathbf{c}^*$, $0 \le \beta \le 1/2$, $0 \le \gamma \le 1$.

1. Introduction

The brownmillerite structure demonstrates one of the most common patterns of anion vacancy order in anion-deficient perovskites.[1,2] The $A_2BB'O_5$ brownmillerite-type structure is described by the $-AO-BO_2-AO-B'O\square-AO-$ ($\square$ = oxygen vacancy) sequence of layers alternating along the 4-fold axis of the perovskite subcell (Figure 1a). Anion vacancies reside in the B′O□ layers and are arranged in rows along the $[110]_p$ direction (subscript p denotes the perovskite subcell). The ordering of anion vacancies reduces the coordination number of the B′ cations down to four, and they adopt a tetrahedral coordination environment. The $B'O_4$ tetrahedra are arranged into tetrahedral chains by corner-sharing. The chains lie parallel to $[110]_p$ and form tetrahedral slabs, sandwiched between two slabs of BO_6 octahedra. The resulting unit cell is orthorhombic with $a \approx a_p\sqrt{2}$, $b \approx 4a_p$, and $c \approx a_p\sqrt{2}$. The B′ and O atoms in the B′O□ layers are displaced from their ideal positions in the perovskite structure. This displacement can be described as a cooperative rotation of the $B'O_4$ tetrahedra in the chains. The rotation of the tetrahedra in opposite directions results in two mirror-related configurations of the tetrahedral chains, which are arbitrarily called "left" (L) and "right" (R) (Figure 1b). The arrangement of the R and L chains between tetrahedral layers (interlayer) and within the tetrahedral layers (intralayer) is the origin of complexity of the brownmillerite-type structures. Three types of brownmillerite structure are generally considered: (a) all tetrahedral chains are of the same type, the structure adopts the *I2mb* space symmetry; (b) layers of R chains alternate with layers of L chains along the *b* axis (interlayer order), the structure adopts the *Pnma* space symmetry; and (c) the R and L chains are randomly distributed, the structure adopts the *Imma* space symmetry. However, it was realized that the L and R chains can be ordered not only in separate layers but also within one layer, thus forming ordered sequences along the *c* axis. A description of possible ordering variants within the layer related to a variation of the relative amount of the R and L chains in the structure and their mutual arrangement was proposed by Lambert et al.[3] using a formalism of (3 + 1)-dimensional crystallography. The ordered pattern of the tetrahedral chains was modeled with step-like occupational modulation functions for the B′ and O atoms in the tetrahedral layers in the frame of the $a \approx a_p\sqrt{2}$, $b \approx 4a_p$, and $c \approx a_p\sqrt{2}$ average unit cell with the $Imma(00\gamma)s00$ superspace group with modulation vector $\mathbf{q} = \gamma\mathbf{c}^*$.[3,4]

The L and R tetrahedral chains differ only by small atomic displacements. The transformation of an L chain to an R chain and vice versa does not change the first coordination spheres and does not noticeably influence the rest of the structure, because the mirror reflection, which is the symmetry element of this transformation, is also a symmetry element of the perovskite matrix. On the basis of these considerations it was concluded that the chains have similar formation energies and can occur in the structure with equal probability. The energy gain causing the ordering of the tetrahedral chains was attributed to the dipole−dipole interaction since dipole moments of equal value but opposite directions, caused by cooperative atomic displacements in the B′O□ layers with respect to the perovskite matrix,[5,6] can be associated to the L and R chains. It was assumed that the

* Corresponding author. E-mail: hans.dhondt@ua.ac.be. Tel: +3232653263. Fax: +3232653257.
† University of Antwerp.
‡ Moscow State University.

(1) Anderson, M. T.; Vaughey, J. T.; Poeppelmeier, K. R. *Chem. Mater.* **1993**, *5*, 151–165.
(2) Abakumov, A. M.; Rozova, M. G.; Antipov, E. V. *Russ. Chem. Rev.,* **2004**, *3*, 847–860.
(3) Lambert, S.; Leligny, H.; Grebille, D.; Pelloquin, D.; Raveau, B. *Chem. Mater.* **2002**, *14*, 1818–1826.
(4) Abakumov, A. M.; Alekseeva, A. M.; Rozova, M. G.; Antipov, E. V.; Lebedev, O. I.; Van Tendeloo, G. *J. Solid State Chem.* **2003**, *174*, 319–328.

10.1021/cm801723b CCC: $40.75
Published on Web 10/25/2008

competition between the inter- and intralayer tetrahedral chain order depends on the separation between the tetrahedral layers and on the magnitude of the atomic displacements, which is reflected by the B′−O−B′ bond angle.[7,8] This consideration was used to explain the tetrahedral chain order in the $A_2MnB'O_5$ (A = Ca, Sr, B′ = Al, Ga) brownmillerites[7,8] and the driving force for the phase transition in $Ca_2Fe_2O_5$.[9] Comparing Sr_2MnGaO_5 and $Sr_2Fe_2O_5$ with other brownmillerite structures, one can realize that the distance between the tetrahedral layers in these two compounds is relatively large (∼8.1 Å in Sr_2MnGaO_5[10] and ∼7.8 Å in $Sr_2Fe_2O_5$[11−15]) and the B′−O−B′ bond angles in both structures deviate strongly from 180°, reflecting significant atomic displacements in the chains (125.7° in Sr_2MnGaO_5[10] and 130.5°−132.6° in $Sr_2Fe_2O_5$[11−15]). From transmission electron microscopy data it is known that the intralayer tetrahedral chain order is realized for Sr_2MnGaO_5, which corresponds to the −L−R−L−R− alternation of chains along the *c* axis ($\gamma = 1/2$).[4] On the basis of the similarity between Sr_2MnGaO_5 and $Sr_2Fe_2O_5$ an intralayer order could be expected also for the latter compound, but in spite of numerous structural studies on $Sr_2Fe_2O_5$ such order was never reported. From the results of neutron powder diffraction and X-ray single crystal diffraction it was reported that $Sr_2Fe_2O_5$ has either the disordered *Imma* structure[11,12,14] or the ordered *I2mb* structure[13,15] with a single type of tetrahedral chains. The disorder in the *Imma* structure was attributed to an irregular alternation of tetrahedral layers consisting of L and R chains so that fragments of the *I2mb* structure occur locally.[11]

In this contribution we report a detailed transmission electron microscopy investigation of $Sr_2Fe_2O_5$ revealing that this compound demonstrates an order of the L and R chains within the tetrahedral layers and different ordered stacking variants of these layers. To describe the locally observed ordered stacking sequences, a general superspace model is proposed, which is then applied to derive the polytypic structures of brownmillerites.

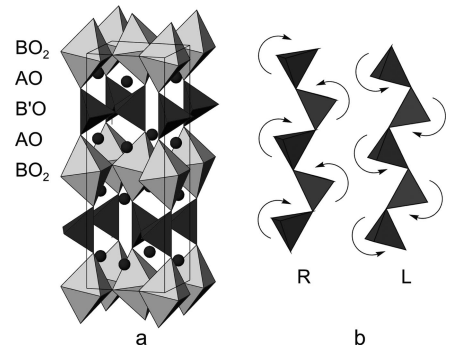

Figure 1. (a) Crystal structure of $A_2BB'O_5$ brownmillerite. The B and B′ cations are situated in the octahedra and tetrahedra, respectively. The A cations are shown as spheres. (b) Two mirror-related configurations of the tetrahedral chains in the brownmillerite structure.

2. Experimental Section

The $Sr_2Fe_2O_5$ sample was prepared from Fe_2O_3 ("Reakhim", "pure for analysis" purity grade) and SrO. SrO was obtained by thermal decomposition of $SrCO_3$ ("Reakhim", "pure for analysis" purity grade) at 1050 °C for 36 h in a dynamic vacuum of 10^{-4} mbar. The required amounts (molar ratio 1:2) of the oxides were mixed in an Ar-filled glovebox, pressed into pellets, placed in alumina crucibles, and sealed into silica tubes with a volume of ∼10 cm^3 evacuated to residual pressure of $\sim 10^{-2}$ mbar. The samples were annealed at 1000 °C for 40 h and then furnace cooled. Alternatively, $Sr_2Fe_2O_5$ was prepared by annealing of the $SrFeO_{2.9}$ precursor in a dynamic vacuum. The precursor was synthesized from stoichiometric amounts of $SrCO_3$ and Fe_2O_3 by annealing at 1000 °C in air. The pellet of precursor was placed in an alumina crucible and annealed in a silica tube at 800 °C in a dynamic vacuum of 2×10^{-5} mbar. The sample was kept under vacuum while cooled in the furnace.

The samples for transmission electron microscopy investigation were prepared by crushing the powder sample in ethanol and depositing it on a holey carbon grid. Electron diffraction (ED) studies were performed using a Philips CM20 microscope, and for high resolution transmission electron microscopy (HRTEM) a JEOL 4000EX microscope was used. The theoretical HRTEM images were calculated by means of the Jems software. The JANA2000 program package was used for handling the superspace structure model.[16]

3. Results

3.1. X-ray Powder Diffraction. Both synthesis techniques (annealings in sealed silica tube and in a dynamic vacuum) resulted in the formation of a single phase $Sr_2Fe_2O_5$ sample. The powder XRD pattern (Figure 2) was indexed on a body-centered orthorhombic unit cell with the lattice parameters $a = 5.5298(4)$ Å, $b = 15.5875(12)$ Å, and $c = 5.6687(4)$ Å. The lattice parameters and intensity distribution on the powder XRD pattern are characteristic for a brownmillerite-type structure. The analysis of the reflection conditions suggests two possible space groups *Imma* or *I2mb*, in agreement with those published before for the $Sr_2Fe_2O_5$ structure.[11−15]

3.2. Electron Diffraction. The ED patterns along the main zone axes of $Sr_2Fe_2O_5$ are shown in Figure 3. The brightest reflections in all the ED patterns can be indexed on a body

(5) Krekels, T.; Milat, O.; Van Tendeloo, S.; Amelinckx, G.; Babu, T. G. N.; Wright, A. J.; Greaves, C. *J. Solid State Chem.* **1993**, *105*, 313–335.
(6) Milat, O.; Krekels, T.; Van Tendeloo, G.; Amelinckx, S. *J. Phys. I France* **1993**, *3*, 1219–1234.
(7) Abakumov, A. M.; Kalyuzhnaya, A. S.; Rozova, M. G.; Antipov, E. V.; Hadermann, J.; Van Tendeloo, G. *Solid State Sci.* **2005**, *7*, 801–811.
(8) Hadermann, J.; Abakumov, A. M.; D'Hondt, H.; Kalyuzhnaya, A. S.; Rozova, M. G.; Markina, M. M.; Mikheev, M. G.; Tristan, N.; Klingeler, R.; Büchner, B.; Antipov, E. V. *J. Mater. Chem.* **2007**, *17*, 692–698.
(9) Krüger, H.; Kahlenberg, V. *Acta Crystallogr., Sect. B* **2005**, *656*, 662.
(10) Pomyakushin, V. Yu.; Balagurov, A. M.; Elzhov, T. V.; Sheptyakov, D. V. P.; Fisher, P.; Khomskii, D. I.; Yushankhai, V. Yu.; Abakumov, A. M.; Rozova, M. G.; Antipov, E. V.; Lobanov, M. V.; Billinge, S. J. L. *Phys. Rev. B* **2002**, *656*, 184412.
(11) Greaves, C.; Jacobson, A. J.; Tofield, B. C.; Fender, B. E. F. *Acta Crystallogr.* **1975**, *B31*, 641–646.
(12) Berastegui, P.; Eriksson, S.-G.; Hull, S. *Mater. Res. Bull.* **1999**, *34*, 303–314.
(13) Schmidt, M.; Campbell, S. J. *J. Solid State Chem.* **1999**, *156*, 292–304.
(14) Hodges, J. P.; Short, S.; Jorgensen, J. D.; Xiong, X.; Dabrowski, B.; Mini, S. M.; Kimball, C. W. *J. Solid State Chem.* **2000**, *151*, 190–209.
(15) Harder, M.; Müller-Buschbaum, H. *Z. Anorg. Allg. Chem.* **1980**, *464*, 169–175.
(16) Petricek, V. Dusek, M. *The Crystallographic Computing System JANA2000*; Institute of Physics: Praha, Czech Republic, 2000.

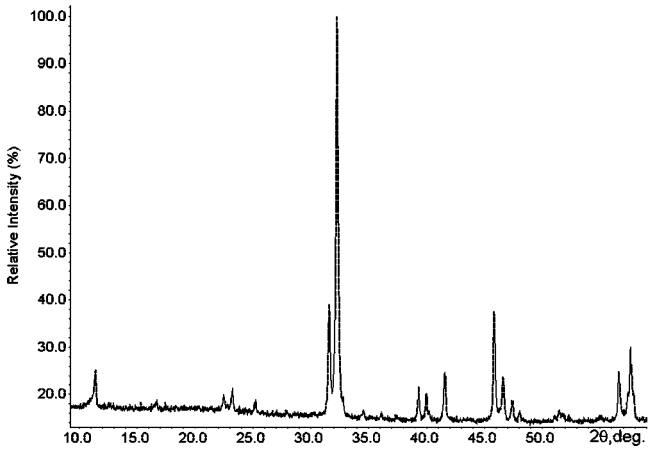

Figure 2. X-ray diffraction pattern of $Sr_2Fe_2O_5$.

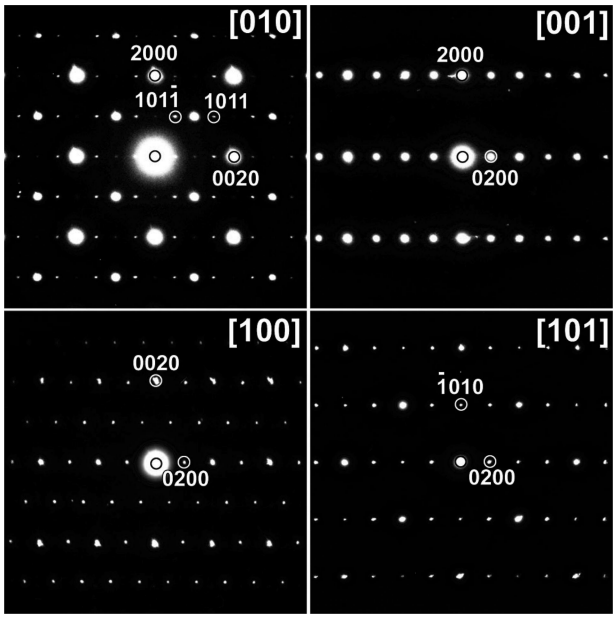

Figure 3. Electron diffraction patterns of $Sr_2Fe_2O_5$ along the main zone axes.

centered orthorhombic unit cell with the cell parameters determined from the powder XRD pattern. These brightest reflections are typical for a brownmillerite-type structure and belong to the average structure. Except for these basic reflections, a set of weaker reflections is visible on the [010] ED pattern. These satellite reflections are situated at the $h0(l \pm 1/2)$ positions and require doubling of the c parameter to be indexed. Careful digitized measurement of the reflection positions showed that on some [010] ED patterns the satellite reflections are slightly displaced along $\mathbf{c}^*$ from the ideal $h0(l \pm 1/2)$ positions indicating incommensurability.

Satellite reflections were not only found on the [010] ED patterns but also along the [102] zone axis (Figure 4). Frequently, dense sets of satellite reflections and diffuse intensity lines were observed along the $[h\ 0\ l/2] \pm \beta\mathbf{b}^*$ reciprocal lattice rows (Figure 4a). Regions were found where the satellites form discrete sets adopting different positions along the $\mathbf{b}^*$ axis as shown in Figure 4b,c. The ED patterns can be completely indexed with four *hklm* indexes given by the diffraction vector $\mathbf{g} = h\mathbf{a}^* + k\mathbf{b}^* + l\mathbf{c}^* + m\mathbf{q}$, where $\mathbf{q} = \beta\mathbf{b}^* + \gamma\mathbf{c}^*$. The γ value varies slightly for different crystallites but stays very close to 1/2. For the [010] ED pattern in Figure 3 the γ value is exactly equal to 1/2 as it can be seen from the absence of splitting of the satellites with $m = \pm 2$. Among other compounds with the brownmillerite-type structure, several examples can be found where the γ component adopts values significantly different from 1/2 ($Ca_2Co_{2-x}Al_xO_5$: $\gamma = 5/8$ and 2/3;[3] $Ca_2Fe_2O_5$ ($T = 1100$ K): $\gamma = 0.588$;[9] $Ca_2Al_2O_5$ ($T = 1090$ K): $\gamma = 0.595$;[17] $Ba_2In_2O_5$: $\gamma = 2/3$[18]). Since in our case the deviation of γ from 1/2 is less than 1%, we prefer to consider $\gamma = 1/2$ for $Sr_2Fe_2O_5$ as a particular commensurate case of the generally incommensurate structure.

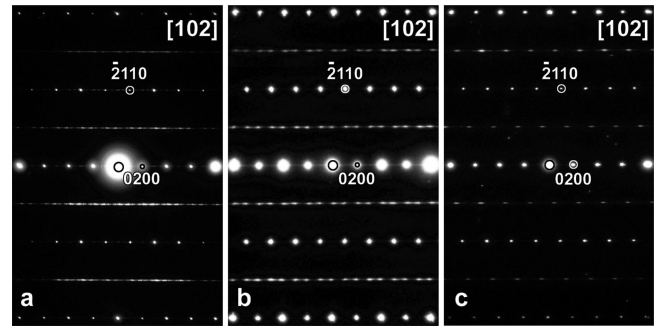

Figure 4. [102] ED patterns from different crystallites of $Sr_2Fe_2O_5$ showing diffuse intensity lines at the $[h\ 0\ l/2] \pm \beta\mathbf{b}^*$ positions (a) and discrete satellite reflections corresponding to $\beta \approx 1/8$ (b) and $\beta = 1/2$ (c).

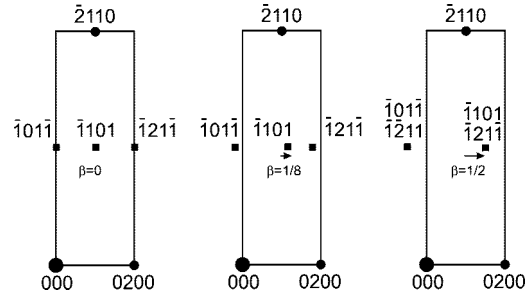

Figure 5. Indexation schemes of the [102] ED patterns for the $\beta = 0$, $\beta = 1/8$, and $\beta = 1/2$. The rectangular box is drawn as a guide to the eye.

The β component can be determined from the position of the satellites on the [102] ED patterns. The satellite reflections in the [102] ED pattern arise from the intersection of the rows of first-order satellites by the (102)* reciprocal lattice plane as explained in ref 4. The satellites with $k = 2n$ in the $h = 1$ row can be indexed as $\bar{1}k1\bar{1}$, and the satellites with $k = 2n+1$ can be indexed as $\bar{1}k01$ (see the indexation scheme in Figure 5). It should be noted that the $\mathbf{q}$ vector is inclined with respect to the (102)* reciprocal lattice plane and that only the $\beta\mathbf{b}^*$ component lies in the plane. The cases with $\beta \approx 1/8$ and $\beta = 1/2$ correspond to the experimental ED patterns in Figure 4b,c, respectively. The indexation schemes for $\beta = 0$, 1/8, and 1/2 are shown in Figure 5. Thus, the reciprocal space of $Sr_2Fe_2O_5$ can be completely described with a single modulation vector, containing two components. For this particular sample the component along $\mathbf{b}^*$ varies in

(17) Lazic, B.; Krüger, H.; Kahlenberg, V.; Konzett, J.; Kaindl, R. *Acta Crystallogr.* **2008**, *B64*, 417–425.
(18) Berastegui, P.; Hull, S.; Garcia-Garcia, F. J.; Eriksson, S.-G. *J. Solid State Chem.* **2002**, *164*, 119–130.

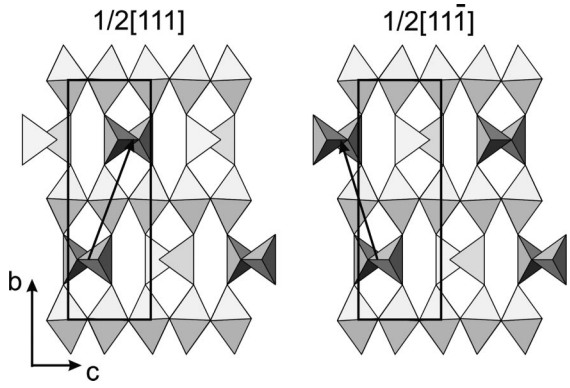

Figure 6. Scheme of displacements of the tetrahedral layers in the brownmillerite structure over the 1/2[111] or 1/2[11$\bar{1}$] vectors (shown by arrows). The R and L tetrahedral chains are shown in projection by different shading. The unit cell indicated is that of the average brownmillerite structure.

Table 1. Atomic Coordinates and Crenel Function Parameters for $Sr_2Fe_2O_5$ (a = 5.5298(4) Å, b = 15.5875(12) Å, c = 5.6687(4) Å, q = βb* + γc*, SSG $I2/m(0\beta\gamma)0s$)[a]

atom	x_1	x_2	x_3
Sr1	1/2	0.1093	0.5159
Sr2	1/2	0.3907	0.5159
Fe1	0	0	1/2
Fe2	0	1/2	1/2
Fe3[b]	0.4555	0.25	0.0678
O1	0.25	−0.0077	0.75
O2	0	0.1402	0.5490
O3	0	0.3598	0.5490
O4[b]	0.6245	0.25	0.3579

[a] The atomic coordinates are transformed from those given in ref 12. [b] Occupational modulation is defined by crenel function with $x_4{}^0 = (1 - \gamma)/4 + \gamma x_3$, $\Delta = 1/2$.

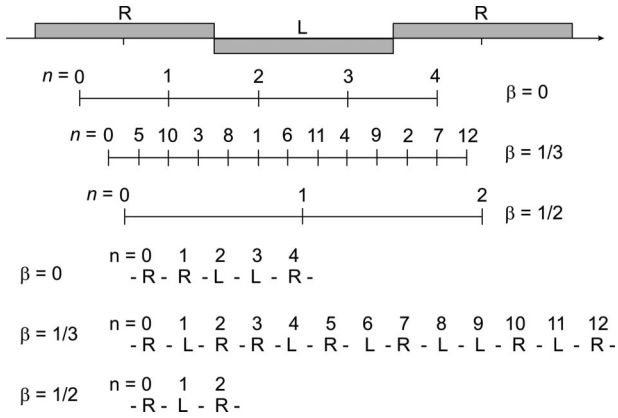

Figure 7. Positions of the $t = 0$ section for the tetrahedral layer with number n with respect to the crenel domains and the sequences of the tetrahedral chains along the [111] direction of the average structure for $\beta = 0$, 1/3, and 1/2.

a wide range limited by $\beta = 0$ and $\beta = 1/2$, whereas the component along **c*** varies in a very narrow range near $\gamma = 1/2$.

In the particular case of $\beta = 0$, the reflection conditions $hklm$, $h + k + l = 2n$; $hk00$, $h, k = 2n$; and $0klm$: $m = 2n$ derived from the ED patterns are compatible with the (3 + 1)D superspace group $Imma(00\gamma)s00$, used earlier for modeling tetrahedral chain order in brownmillerites.[2−4] In the general case that $\beta \neq 0$, the symmetry should be decreased down to monoclinic. The $I2/m(0\beta\gamma)0s$ (3 + 1)D superspace group (unique axis a, No. 12.2 in ref 19, $B2/m(\alpha'\beta'0)0s$, **a′** = **b** − **c**, **b′** = **c**, **c′** = **a**, $\alpha' = \beta - \gamma$, $\beta' = \gamma$), which is a subgroup of $Imma(00\gamma)s00$, can be used for the $\beta \neq 0$ case. This superspace group matches with the $hklm$, $h + k + l = 2n$; $0klm$, $m = 2n$ reflection conditions experimentally observed in $Sr_2Fe_2O_5$, but the $hk00$, $h, k = 2n$ reflection condition is not imposed by any symmetry element of this group. Following Krekels et al.[5] it can be shown that this extra reflection condition arises from the symmetry properties of the tetrahedral chain superstructure and the stacking of the tetrahedral layers assuming the perfect −L−R−L−R− intralayer tetrahedral chain order (see Appendix).

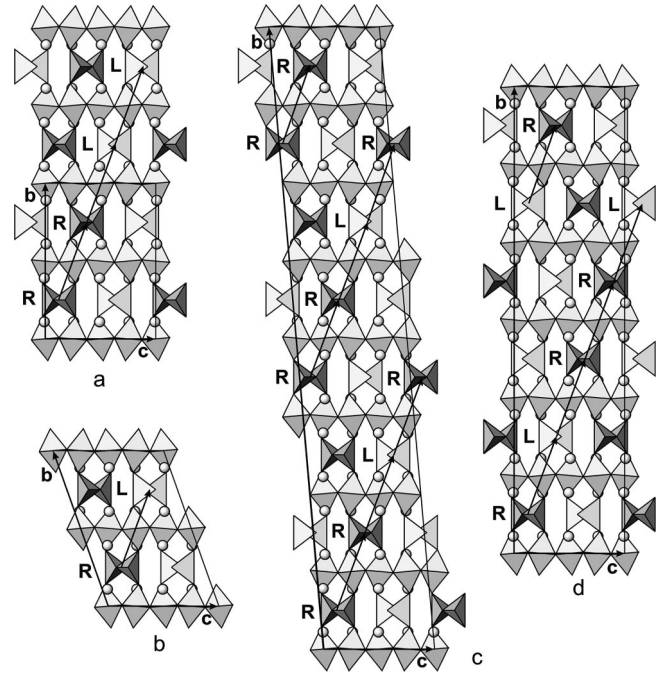

Figure 8. Commensurate structures with the stacking sequences of tetrahedral layers for $\beta = 0$ (a), 1/2 (b), 1/8 (c), 1/3 (d). The 1/2[111] vector of the brownmillerite subcell is shown by arrows.

Table 2. Three-Dimensional Space Groups for Stacking Sequences of Tetrahedral Layers in Brownmillerites Derived from the $I2/m(0\beta\gamma)0s$ Superspace Group for Different t, Rational β, and $\gamma = 1/2$ Values[a]

$\beta = r/s$	$t = \tau/4s$	$t = (2\tau + 1)/8s$	$t = \tau/2s$	$t = (2\tau + 1)/4s$	general t
$r = 0$			$Pcmb$	$Pcma$	$Pcm2_1$
r = any integer, $s = 2v + 1$	$P2/c$	$P2_1/c$			Pc
$r = 2\mu + 1$, $s = 4v$[b]			$P2/c$	$P2_1/c$	Pc
$r = 4\mu - 3$, $s = 4v + 2$[b]			$C2/c$		Cc
$r = 4\mu - 1$, $s = 4v + 2$[b]			$I2/c$		Ic

[a] The space groups for the $\beta = 0$ case are derived from the $Imma(00\gamma)s00$ superspace group. r, s, ν, μ, and τ are integers. The unique axis for the monoclinic structures is a. [b] The transformation **a″** = **a**, **b″** = 1/2(**b** − **c**), **c″** = **c** is applied to the 3D unit cell.

3.3. Models for Tetrahedral Chain Order. We shall assume that the satellite reflections on the ED patterns of $Sr_2Fe_2O_5$ arise from an ordered arrangement of the tetrahedral chains in the L and R configurations. Two levels of such order can be distinguished:

(1) The ordered alternation of L and R chains within the tetrahedral layers, associated with the γ-component of the modulation vector. The sharpness of the satellite reflections on the [010] ED pattern (Figure 3) and the orientation of the diffuse intensity lines on the [102] ED pattern (Figure 4a) along the normal to the tetrahedral layers reflects that long-range order is established within the layers.

(2) The adjacent tetrahedral layers are displaced with respect to each other by 1/2[1 1 ± 1] vectors which is a translation of the average brownmillerite structure. The layers displaced either by 1/2[111] or by 1/2[11$\bar{1}$] vectors (Figure 6) can form ordered stacking sequences associated with the β-component of the modulation vector. The observation of discrete satellites on the [102] ED patterns (Figure 4b,c) suggests that such ordered sequences are present at least locally, and the diffuse intensity lines on these patterns arise from the areas where long-range order between the layers is absent.

Following the approach given in ref 20, the stacking sequence of the tetrahedral layers will be directly inferred from the β-component of the modulation vector. The superspace construction previously proposed by Lambert et al.[3] for modeling the alternation of the L and R chains within the tetrahedral layers can be adapted to model also the stacking sequence of the tetrahedral layers by choosing a different modulation vector, the oblique $\mathbf{q} = \beta\mathbf{b}^* + \gamma\mathbf{c}^*$, and decreasing the symmetry from the *Imma*(00γ)*s*00 space group to its subgroup *I*2/*m*(0$\beta\gamma$)0*s*. The atomic coordinates of the $Sr_2Fe_2O_5$ structure reported by Berastegui et al.[12] (in the *cba* setting, *Icmm* space group) were first transformed from the *Imma* to *I*2/*m* space group. The tetrahedral layers in the transformed structure consist of one Fe and one O position at (x_1, 1/4, x_3). The occupancy modulation resulting in an ordered alternation of the R and L chains along the *c* axis within the layer is described with a step-like occupational modulation function (crenel function), which is defined by the width of the step Δ in x_4 and its midpoint x_4^0. Atoms within the Δ interval have an occupancy factor equal to 1, otherwise the occupancy factor is equal to 0.[21,22] The parameters of the crenel domains for the Fe and O positions resulting in either an R or an L chain at a certain place in the structure are $x_4^0 = (1 - \gamma)/4 + \gamma x_3$, and $\Delta = 1/2$ (see[2−4] for the derivation). The (x_1, x_2, x_3) coordinates of the atomic positions in the average structure and the corresponding parameters of the crenel domains are given in Table 1. To derive the stacking of the tetrahedral layers one should consider the positions of the sequence of the R and L crenel domains with respect to the section of superspace by the R_3 hyperplane at $t = 0$ taking into account the *n*/2[111] shift when going from layer to layer along the *b* axis, where *n* is the sequential number of the layer starting from $n = 0$ for the layer with ($x_{1,0}$, $x_{2,0}$, $x_{3,0}$), $x_{2,0} = 1/4$. The tetrahedral chain consisting of the Fe3 and O4 atoms with ($x_{1,0}$, $x_{2,0}$, $x_{3,0}$) coordinates as in Table 1 (arbitrarily named an R chain) can be chosen as a reference and a displacement t_n with respect to $t = 0$ of the center of the crenel domains of the Fe3 and O4 atoms for this chain in the *n*th layer can be calculated as a function of *n* and β. This displacement is given by $t_n = x_4^0 - \beta x_{2,n} - \gamma x_{3,n}$, where $x_{2,n} = 1/4 + n/2$, $x_{3,n} = x_{3,0} + n/2$. Taking into account that $x_4^0 = (1 - \gamma)/4 + \gamma x_{3,0}$, one can get $t_n = 1/4[1 - (2n + 1)(\beta + \gamma)]$. For simplicity, further consideration will be performed for $\gamma = 1/2$ since most of the ED patterns do not demonstrate a noticeable deviation from this commensurate value. Positions of the $t = 0$ section for the tetrahedral layer with number *n* with respect to the crenel domains and the sequences of the tetrahedral chains along the [111] direction of the average structure for $\beta = 0$, 1/3, and 1/2 are shown in Figure 7. The obtained 3D structure models are shown in Figure 8. It should be noted that the model can be adapted to an arbitrary *t*-section by an application of the necessary "phase shift" ϕ along the *t*-axis.

Three-dimensional space groups can be derived from the *I*2/*m*(0$\beta\gamma$)0*s* (3 + 1)D superspace group for cases with commensurate modulations corresponding to $\beta = r/s$ (r,s = integers) for different *t* values. The list of space groups in case of $\gamma = 1/2$ is given in Table 2. If $r = 2n + 1$ and $s = 2n$, the [0, *s*/2, 1] translation of the average structure becomes a [0, 1/2, 1/2] translation of the supercell, and a $\mathbf{a}'' = \mathbf{a}$, $\mathbf{b}'' = 1/2(\mathbf{b} - \mathbf{c})$, $\mathbf{c}'' = \mathbf{c}$ transformation should be applied to the 3D unit cell to achieve a conventional setting (unique axis *a*). In the case of $\beta = 0$, the three-dimensional space groups are derived from the *Imma*(00γ)*s*00 superspace group.

3.4. High-Resolution Electron Microscopy. To visualize the stacking sequence of the tetrahedral layers, a zone axis is needed along which the L and R chains demonstrate different projected potentials. It was found in ref 5 that the [102] zone axis is a good viewing direction to distinguish between the different tetrahedral chains. Along this direction the tetrahedral FeO layers appear as bright dots, whereas the other layers are represented as lines running perpendicular to the [010] direction. The tetrahedral layers consisting of chains of the same type produce a repeat period along the layer equal to ≈2.4 Å, whereas a doubled repeat period of ≈4.8 Å is related to the layers with −L−R−L−R− alternation of chains along the *c* axis within the layer. This will be further elaborated and confirmed by comparing image simulations based on the proposed structure models for the different tetrahedral chain orders with the experimental HREM images. The arrays of 4.8 Å separated dots in two neighboring FeO layers are shifted with respect to each other by a component of the 1/2[111] displacement vector which is normal to the viewing direction, which corresponds approximately to 1/3 of the interdot distance. The HREM image along [102] (Figure 9) shows an area where the stacking sequence corresponds to the orthorhombic *Pcmb* structure (Figure 8a). The satellite reflections on a Fourier transform of this image (see inset in Figure 9) are located at the positions corresponding to $\beta = 0$. A calculated HREM

(19) Janssen, T.; Janner, A.; Looijenga-Vos, A.; de Wolff, P. M. In *International Tables for Crystallography*; Wilson, A. J., Ed.; Kluwer Academic Publishers: Dordrecht, 1999; Vol. C, pp 899−947.
(20) Perez-Mato, J. M.; Zakhour-Nakhl, M.; Weill, F.; Darriet, J. *J. Mater. Chem.* **1999**, *9*, 2795–2808.
(21) van de Lee, A.; Evain, M.; Monconduit, L.; Brec, R.; Rouxel, J.; Petricek, V. *Acta Crystallogr.* **1994**, *B50*, B50–128.
(22) Petricek, V.; van der Lee, A.; Evain, M. *Acta Crystallogr.* **1995**, *A51*, 529–535.

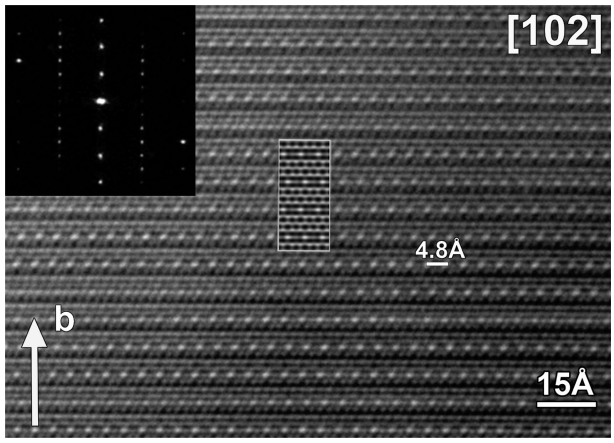

Figure 9. [102] HREM image of $Sr_2Fe_2O_5$ showing an area of the ordered orthorhombic structure with $\beta = 0$ and *Pcmb* space symmetry. The Fourier transform is shown as an inset at the top left corner. The calculated HREM image ($\Delta f = -200$ Å, $t = 50$ Å) is indicated by a white border and is in good agreement with the experimental image.

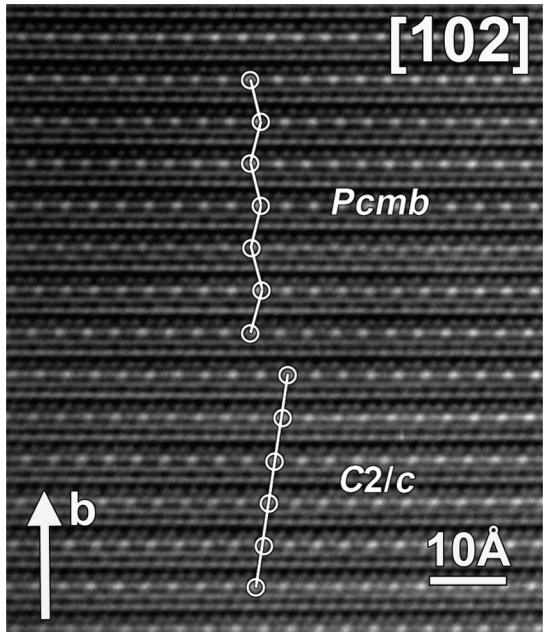

Figure 10. [102] HREM image showing an intergrowth of the orthorhombic $\beta = 0$ (*Pcmb*) and monoclinic $\beta = 1/2$ (*C2/c*) structures.

image, using the model described above, shows good agreement with the experimental HREM image ($\Delta f = -200$ Å, $t = 50$Å) and is put as an inset in Figure 9.

The [102] HREM image in Figure 10 demonstrates an intergrowth of the orthorhombic *Pcmb* ($\beta = 0$, Figure 8a) and monoclinic *C2/c* ($\beta = 1/2$, Figure 8b) structures. If these structures are considered in terms of the displacements of the tetrahedral layers; the displacement over 1/2[111] vector alternates with the 1/2[11$\bar{1}$] one for the *Pcmb* structure, whereas for the *C2/c* structure the cumulative 1/2[11$\bar{1}$] displacement occurs. The difference in the displacement sequence is reflected on the HREM image by a staggered arrangement of the bright dots in the domain of the *Pcmb* structure and an oblique arrangement of the bright dots in the domain of the *C2/c* structure. It should be noted that the monoclinic structure with a cumulative displacement of the tetrahedral layers as in the *C2/c* structure was also observed in the $La_{1.5}Sr_{0.5}Mn_2O_5$ brownmillerite.[23]

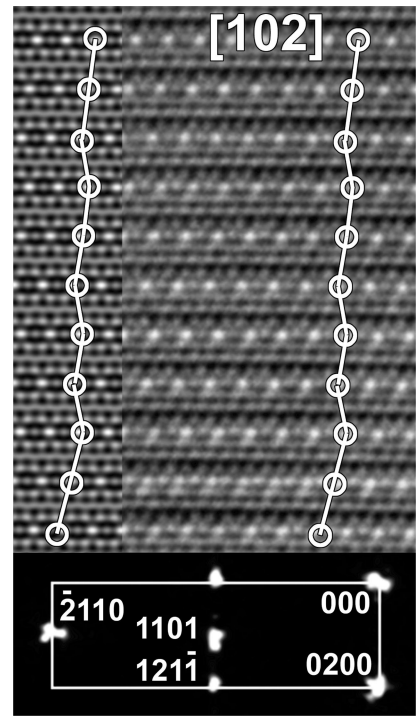

Figure 11. [102] HREM image showing a local area of the monoclinic $\beta = 1/8$ (*P2/c*) structure. The Fourier transform is shown at the bottom. The left side shows the calculated HREM image ($\Delta f = -200$ Å, $t = 50$ Å) according to the model from Figure 8c which is in good agreement with the experimental image.

Local areas of the monoclinic $\beta = 1/8$ structure with the space symmetry *P2/c* were also observed. On the [102]

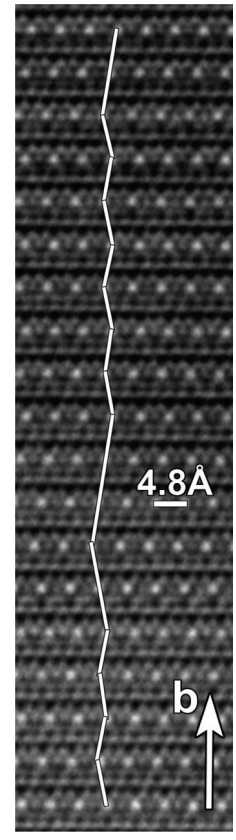

Figure 12. [102] HREM image showing disordered stacking sequence of the tetrahedral layers.

HREM image (Figure 11) the experimentally observed arrangement of the bright dots can be compared with the arrangement calculated with the model shown in Figure 8c. The satellite positions on the Fourier transform of the image (bottom of Figure 11) agree with the $\beta = 1/8$ value.

Diffuse intensity lines on the [102] ED patterns in Figure 4a demonstrate that disorder is also present in the stacking sequence of the tetrahedral layers. The HREM image of disordered stacking of the tetrahedral layers is shown in Figure 12, where the regions of the staggered and oblique arrangements of dots are marked with a white line.

4. Discussion

The transmission electron microscopy investigation clearly revealed that the L and R tetrahedral chains in the $Sr_2Fe_2O_5$ structure form perfect two-dimensional order within the tetrahedral layers according to the −L−R−L−R− sequence. Such an arrangement of the tetrahedral chains within the layer looks most favorable for the mutual compensation of the opposite dipoles associated with the L and R chains because it provides the shortest separation between the chains of different types. In contrast to that, no significant energy gain is related to the ordering of the tetrahedral layers because changing the stacking sequence by a mutual displacement of the layers does not alter the nearest-neighbor separations between the L and R chains (see Figure 6). This causes the simultaneous presence of areas with different ordered stacking sequences of the layers and local areas of disordered stacking. This scheme of anion-vacancy ordering in $Sr_2Fe_2O_5$ is different from that proposed by Greaves et al.,[11] where the tetrahedral layers are considered as consisting of either L or R chains and domains of the *I*2*mb* structure are locally present. The observed arrangement of the tetrahedral chains in $Sr_2Fe_2O_5$ allows ruling out the *I*2*mb* structure as a model for tetrahedral chain order and confirms the correctness of the disordered *Imma* structure when derived by such bulk technique of structure characterization as neutron powder diffraction. However, the ordered stacking sequences can be observed over relatively large local areas (such as the area of *Pcmb* structure in Figure 9) using high resolution electron microscopy. The size of such ordered areas should strongly depend on the conditions of thermal treatment of the sample, and one can expect that long-range ordered stacking sequences of tetrahedral layers could be obtained by finding appropriate cooling regimes.

Acknowledgment. This work was supported by Russian Foundation of Basic Research (RFBR Grants 07-03-00664-a, 06-03-90168-a, and 05-03-34812-MIF-a). The work was supported in part by the IAP VI program of the Belgian government.

Appendix

The structure factor F_0 can be assigned to the FeO tetrahedral layer consisting of a perfect −L−R−L−R− tetrahedral chain sequence. Being projected along the [001] direction, the projected structure factors of the L and R chains are equal, $F_L = F_R = F$. Then $F_0 = F(1 + e^{\pi ih})$, where the $e^{\pi ih}$ factor arises from a shift of the tetrahedra with the same projected potential by 1/2**a** along the chains. Taking into account that the tetrahedral layers are related by a 1/2[111] translation of the average brownmillerite structure, the projected structure factor for the spatial arrangement of the tetrahedral chain can be written as $F_P = F(1 + e^{\pi ih})(1 + e^{\pi i(h+k)})$. From this expression it can be seen that $F_P \neq 0$ only if both $h = 2n$ and $k = 2n$.

CM801723B

(23) Casey, P. S.; Barker, D.; Hayward, M. A. *J. Solid State Chem.* **2006**, *179*, 1375–1382.